Retrieval of sea-ice thickness distribution in the Sea of Okhotsk from ALOS/PALSAR backscatter data

Takenobu TOYOTA,[1] Shuji ONO,[2] Kohei CHO,[3] Kay I. OHSHIMA[1]

[1]Institute of Low Temperature Science, Hokkaido University, Sapporo 060-0819, Japan
E-mail: toyota@lowtem.hokudai.ac.jp
[2]Information and Science Techno-System Co., Ltd, Tskuba 305-0032, Japan
[3]Tokai University, Shibuya-ku, Tokyo 151-0063, Japan

ABSTRACT. Although satellite data are useful for obtaining ice-thickness distribution for perennial sea ice or in stable thin-sea-ice areas, they are still largely an unresolved issue for the seasonal ice zone (SIZ). We address this problem using L-band synthetic aperture radar (SAR). In the SIZ, ice-thickness growth is closely related to deformation, so surface roughness is expected to correlate with ice thickness. L-band SAR, suitable for detecting such surface roughness, is a promising tool for obtaining thickness distribution. This idea was supported by an airborne polarimetric and interferometric SAR (Pi-SAR) validation. To extend this result to spaceborne L-band SAR with coarser resolution, we conducted in situ measurements of ice thickness and surface roughness in February 2008 in the southern Sea of Okhotsk with an icebreaker in coordination with the Advanced Land Observing Satellite (ALOS)/ Phased Array-type L-band SAR (PALSAR) orbit. A helicopter-borne laser profiler was used to improve the estimation of surface roughness. It was found that backscatter coefficients (HH) correlated well with ice thickness ($R = 0.86$) and surface roughness ($R = 0.70$), which confirms the possibility of determining ice-thickness distribution in the SIZ. The interannual variation of PALSAR-derived ice-thickness distribution in the southern Sea of Okhotsk is also discussed.

INTRODUCTION

In winter the Sea of Okhotsk is covered with various types of sea ice whose thickness ranges from a few centimeters to several meters (Fukamachi and others, 2006; Uto and others, 2006). Ice thickness plays a crucial role in the heat exchange between the atmosphere and ocean, in particular ice growth processes, and then the climate on a global scale. Therefore ice-thickness distribution is one of the most important parameters for understanding the effect of sea ice on the climate system. Since spaceborne remote sensing is an ideal tool for obtaining data on a global scale, enormous efforts have been made to develop algorithms to retrieve ice-thickness distribution. For relatively thin ice (<0.2 m), the thickness algorithms for coastal polynyas in Arctic and Antarctic regions, combined with US National Oceanic and Atmospheric Administration (NOAA) Advanced Very High Resolution Radiometer (AVHRR) data, were developed (Martin and others, 2004; Tamura and others, 2007). For thick ice (>1 m), the measurement of the freeboard has proven to be effective with the assumption of isostatic balance, from field observations in the Arctic (Comiso and others, 1991) and from satellite altimetry (radar (Laxon and others, 2003) and laser (Kwok and others, 2004, for the Arctic; Zwally and others, 2008, for the Antarctic)). This allowed estimation of the seasonal and interannual variation of ice volumes in the Arctic Ocean (Kwok and Cunningham, 2008). To reduce the uncertainty caused by snow, Kurtz and others (2009) attempted to combine laser altimetry and passive microwave radiometry. However, while the algorithm for level thin ice or thick ice has been explored, relatively thick sea ice (0.2–1 m) in the seasonal ice zone (SIZ) remains a big issue.
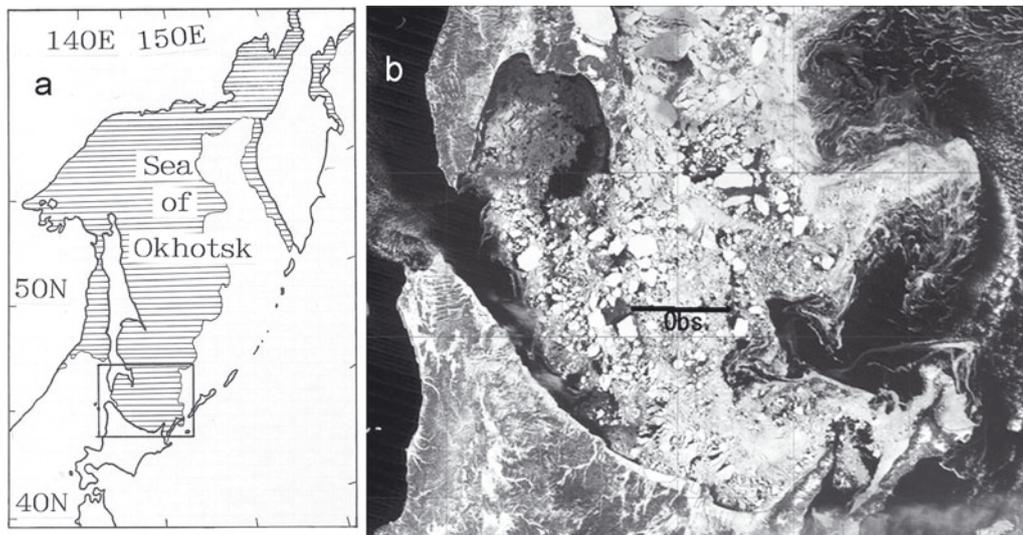
In the SIZ, the degree of surface roughness is expected to be a useful surface property related to ice-thickness distribution because deformation processes in the SIZ, usually accompanied by surface roughness, play an essential role in the development of ice thickness except for landfast sea ice (Worby and others, 1996; Toyota and others, 2007). To extract surface roughness as discussed by Dierking and Busche (2006), L-band synthetic aperture radar (SAR) (0.15–0.30 m wavelength) data appear to be better suited than the C-band (0.03–0.07 m wavelength) data mainly used from satellite SAR so far. This is because L-band is closer to the horizontal scale of surface roughness (~tens of cm to a few meters) than C-band (Lubin and Massom, 2006). To verify this idea, a validation experiment was conducted in the Sea of Okhotsk in February 2005, in coordination with airborne polarimetric and interferometric SAR (Pi-SAR), and promising results were obtained (Toyota and others, 2009). Here we further examine the feasibility of spaceborne L-band SAR (Advanced Land Observing Satellite (ALOS)/Phased Array-type L-band SAR (PALSAR)) with coarser resolution as a tool for estimating ice-thickness distribution in the SIZ. To do this, we conducted concurrent measurements of surface roughness and ice thickness, coordinated with the PALSAR orbit in February 2008. Although the relationship between ice thickness and airborne L-band SAR backscatter data has been presented before (e.g. Nakamura and others, 2005; Kern and others, 2006), this is the first trial to validate it with surface roughness data and apply it to satellite L-band SAR. The main aim of this experiment is to improve the estimation of surface roughness by means of helicopter observations and then to examine the relationship of backscatter data with surface roughness and ice thickness, and the feasibility of spaceborne L-band SAR for estimating the ice-thickness distribution in the SIZ.

METHODS

Background: the previous airborne Pi-SAR experiment

To test the usefulness of L-band SAR for ice-thickness retrieval, measurements of ice thickness and surface

Fig. 1. Ice conditions and location map of the observation on 10 February 2008. (a) Sea-ice extent in the Sea of Okhotsk (based on Japan Meteorological Agency information (http://www.data.kishou.go.jp/kaiyou/db/seaice/okhotsk/okhotsk_extent.html)). (b) MODIS image within the frame of (a) with the observation line (thick solid line).

roughness were conducted in coordination with an airborne Pi-SAR experiment in the Sea of Okhotsk in February 2005 (Toyota and others, 2009). Ice thickness was monitored with a ship-borne electromagnetic induction (EM) system designed for this study area (Uto and others, 2006), while surface topography was measured with a ship-borne supersonic profiler. The surface elevation was obtained by removing the effect of the ship's motion with a low-pass filter (Ishizu and others, 1999), and the surface roughness was calculated by taking the standard deviation of the surface elevation data over a distance of 1 km. Pi-SAR collected fully polarimetric L-band data (1.27 GHz center frequency, i.e. 0.24 m wavelength) with a horizontal resolution of 3 m. As a result, it was determined that the L-band SAR backscatter coefficient (both VV and HH) can be an effective tool to estimate ice thickness because of a good relationship between ice thickness, surface roughness and the backscatter coefficient. This result indicated great promise for the use of satellite L-band SAR data to estimate ice-thickness distribution in the SIZ.

In applying this to a satellite sensor, however, further validation is needed to determine if the strong correlation still holds for the satellite SAR with coarser horizontal resolution. Moreover, as discussed by Toyota and others (2009), there remained some problems with the analytical method of surface roughness as the estimated surface elevation rarely exceeded 0.2 m and appeared to be significantly less than the real topography. They concluded that this underestimation was mainly due to low-pass filtering to obtain the ship's motion. The problem is that the ship's motion can also be affected by ice conditions, so the wavenumber spectrum of the ship's motion and the surface elevation may partly overlap. Thus, the low-pass filtering cannot distinguish sufficiently between the ship's motion and relative surface topography. The use of a helicopter-borne profiler was suggested to solve this problem.
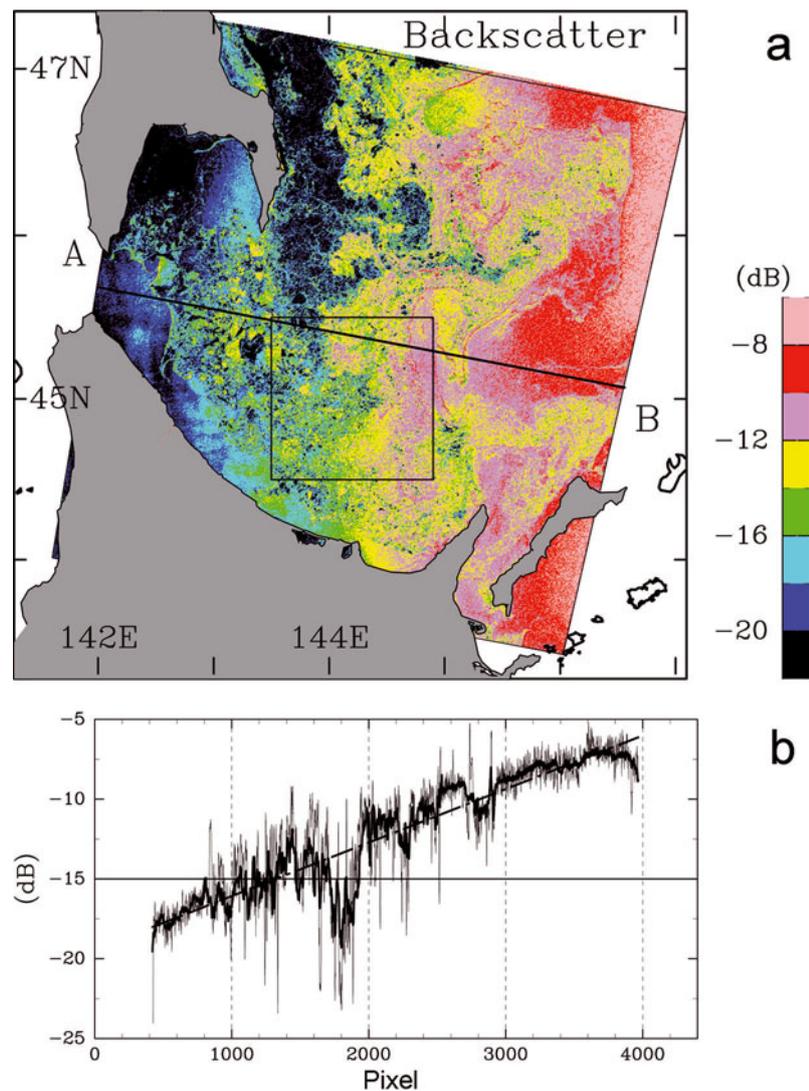
Validation of PALSAR

To extend the above result to the spaceborne L-band SAR data, we conducted in situ measurements with the patrol vessel (P/V) *Soya* in February 2008, coordinated with an overpass of the ALOS/PALSAR. From among the three observation modes of PALSAR (Fine, ScanSAR, Polarimetric), the ScanSAR mode with a single polarization (HH) was chosen for operational reasons. To issue sea-ice information in the southern Sea of Okhotsk on an operational basis from the Japan Coast Guard (JCG), an agreement between the JCG and Japan Aerospace Exploration Agency (JAXA) was established to collect PALSAR data in ScanSAR mode with the HH polarization, due to its wide area (~300 km) coverage. In this mode, the center frequency is 1.27 GHz and the horizontal resolution is 100 m.

Measurements

The in situ observations were carried out on board *Soya* along a longitudinal line ~40 km long from 143.925° E to 144.375° E at 45.2° N in the southern Sea of Okhotsk on 12 February 2008 (Fig. 1). The sea-ice extent in the Sea of Okhotsk (110.69×10^4 km^2) was close to normal (105.08×10^4 km^2 for the period 1971–2000) according to the Japan Meteorological Agency (Fig. 1a), and it is seen in Figure 1b that variable ice conditions were present in the study area.

Ice thickness was measured with the ship-borne monitoring systems of both video and EM. The EM system was the same as used for the Pi-SAR experiment in 2005, while the video monitoring system measurement was done for ice floes which were broken at the bow and turned into side-up positions (Toyota and others, 2004). The measurement accuracy of the EM system is ±0.1 m for undeformed ice (Haas, 2003) and 10% for deformed ice in this region (Toyota and others, 2009). As for the video system, although the measurement accuracy itself is less than a few centimeters, the problems are its representativeness and subjectivity because this is a sporadic measurement. According to Toyota and others (2004), a 10 min running mean (~3 km) gives a general trend of ice thickness that can be regarded as representative. Moreover, since they showed that the difference in mean values between observers is only a few centimeters, it seems to be free from subjectivity. Therefore, the accuracy of this method is considered to be a few centimeters when the 10 min averaged data are

Fig. 2. PALSAR backscatter coefficients observed on 12 February 2008. (a) Geographical distribution in the study area (© JAXA). Square area corresponds to the region depicted in Figure 4. (b) Profile of backscatter coefficient along the A–B cross section in (a), crossing the center of the image. The regression line is shown with a dashed line.
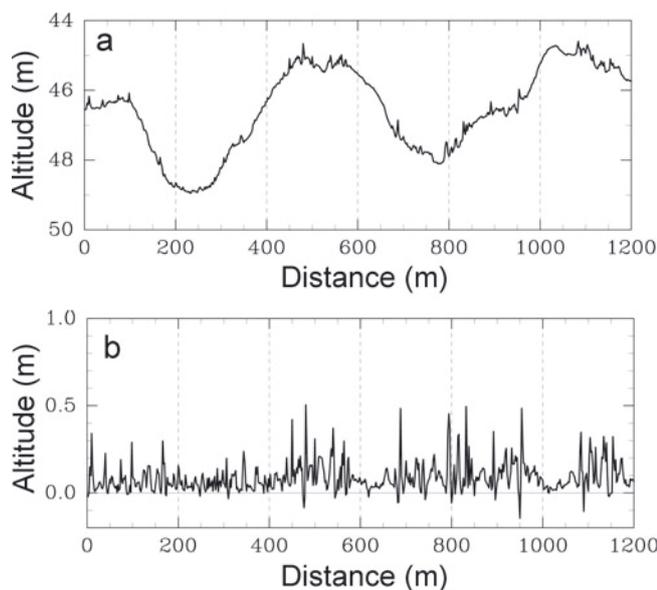
concerned. Since the EM system was not working that day, the video monitoring data were used for validation. It was confirmed that the video data coincide with the EM data for the Okhotsk sea ice except for significantly ridged ice (Toyota, 2009), so they are deemed a useful alternative to EM for validation. The total number of samples along the observation line (Fig. 1b: ~35 km) was 131 (one per 0.27 km on average).

A helicopter-borne laser profiler (RIEGL, LD90-3100HS) was used to improve the accuracy of surface roughness, as suggested by Toyota and others (2009). As a helicopter observation is free from the effect of ice surface conditions, we can expect it to become easier to discern surface topography from the vertical motion of the helicopter in the time series of the profiles. Due to cloudy conditions at the observation time of PALSAR (1004 h local sidereal time (LST)), the helicopter operation was started at 1400 h. For the measurement, a downward-looking profiler was attached to a pole extended through the door of the helicopter. The helicopter flew along the cruise track at an altitude of ~50 m (Fig. 4, further below), and the profiler recorded the height above the surface at 10 Hz (i.e. 2 m spatial resolution). During the flight, surface conditions beneath the helicopter were also monitored with a high-resolution video camera through the other side of the door. The images obtained were used to distinguish between sea-ice and open-water areas. In fact, whereas a heliborne profiler measures the roughness of the snow surface, L-band SAR backscatter corresponds to the snow/ice interface roughness. Even so, our measurement is still valid since Andreas and others (1993) reported that snow surface roughness is strongly correlated with snow/ice interface roughness for Antarctic sea ice.

Analytical procedures

The distribution of PALSAR backscatter coefficient is shown in Figure 2a, where the satellite path is on the eastern side of the image (north-northeast to south-southwest) and the incident angle ranges from 18° to 43° from near to far. The figure indicates that backscatter depends significantly on the incident angle. Figure 2b shows the profile of backscatter coefficients along the A–B cross section in Figure 2a with a regression line derived by a least-square method. To remove the bias caused by the incident angle, the backscatter data at each pixel were normalized to that at the incidence angle (30.4°) of the center of the image using the regression obtained in Figure 2b.

Fig. 3. Example of the time series of heliborne laser profiling data, obtained from 1408 to 1409 h on 12 February 2008. (a) Raw data (b) Estimated surface elevation.

In estimating surface roughness from the laser data, we adopted the same procedure as was used for the Pi-SAR experiment. To extract surface elevation from airborne laser profiles in the polar pack ice, the method of Hibler (1972) which determines a sea level by connecting minimum points is often used (e.g. Comiso and others, 1991). However, in our case where surface topography is relatively small and sometimes comparable to the measurement accuracy (∼a few centimeters), our statistical procedure seems to work more effectively. Although the sampling interval (∼2 m) for heliborne measurement is coarser than the interval of 0.5 m for shipborne measurement, it is found that the accuracy was much improved. An example is shown in Figure 3. Since the variation of height due to the heli-operation had quite different scales from that due to surface topography in both magnitude and time (Fig. 3a), low-pass filtering worked more effectively to extract surface topography compared with the shipborne profiles. The estimated surface elevation ranged from 0.1 to 0.5 m (Fig. 3b) and seems to match well with the ridge sail height estimated by visual observation from the ship.

The difference in observation time among SAR, ice thickness and surface roughness is also an important issue since in this area the southward ocean current is as high as a few tens of centimeters per second (Ohshima and others, 2002) and ice conditions are variable (Fig. 1b). Along the observation line, the shipborne and heliborne measurements were conducted from 0700 to 1600 h and from 1401 to 1445 h LST, respectively. Thus the maximum time difference is 6 hours, corresponding to several kilometers. To correct this, the ice-drift speed was estimated using the video images monitored from the helicopter. We checked the location and time of the ship trails which appeared in the video images and calculated their difference from the shipborne GPS record. The estimated ice-drift speed was $(u, v) = (0.163, -0.188)$ m s^{-1} near the center of the observation line and $(u, v) = (0.178, -0.196)$ m s^{-1} near the eastern edge. Since these two values are very close, the averaged value (0.17, −0.19) m s^{-1} was used, assuming that the drift speed was

invariant. The drift speed due to wind forcing is estimated as $(0.13, -0.02)$ m s^{-1}, assuming that sea ice drifts at a rate of 2% of wind (Kimura and Wakatsuchi, 1999). Therefore the ocean current is estimated as $(0.04, -0.17)$ m s^{-1}, which almost coincides with the value reported by Ohshima and others (2002). With this ice-drift speed and the difference of time at each point, we located the pixels on the backscatter map that should be used for validation (Fig. 4).
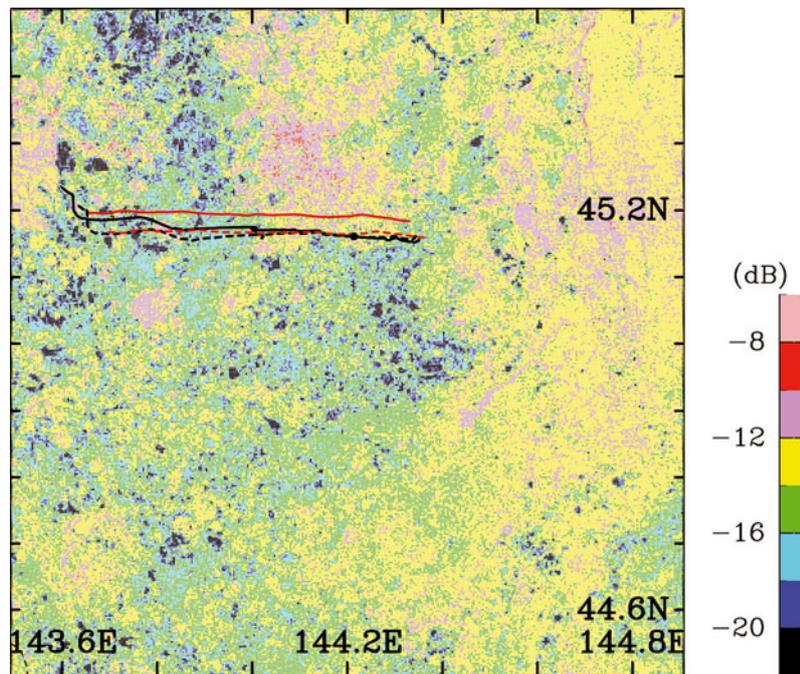
RESULTS

To compare SAR backscatter with ice thickness and surface roughness along each observation line in Figure 4, we sectioned these observation lines into segments every 0.025° in the longitudinal direction (∼2 km), and averaged the data for each segment. Although the length of segment might be too large compared with the horizontal resolution of SAR, we selected this value so as to contain as many thickness data as possible for representativeness. Of the 18 segments in total, 4 segments where the number of ice-thickness data was less than three and the 2 segments where open water dominated were excluded from the analysis of ice thickness. As for the surface roughness, the 4 segments where open water dominated were excluded. As a result, it was found that backscatter has a significant correlation with both ice thickness and surface roughness at >99% level (Fig. 5). The correlation coefficient is 0.86 between ice thickness and backscatter, and 0.70 between backscatter and surface roughness. From Figure 5a the regression line is estimated as

$$H_i = 0.047\mathrm{BS} + 1.012 \qquad (1)$$

with a root-mean-square (rms) error of 0.04 m, where H_i is the ice thickness (m) and BS is the normalized backscatter coefficient at HH polarization (dB). Since the rms error is comparable to the measurement accuracy of the video system, the error from the regression can be explained mainly by the measurement error, indicating the validity of the regression. This result supports our hypothesis that the L-band SAR data correspond well with surface roughness and therefore L-band SAR has a good correlation with ice thickness. However, it should be noted that H_i in Equation (1) is the thickness of less deformed ice due to the measurement method. To estimate the ice thickness including significantly deformed ice, the slope of the regression may be somewhat larger, especially for ice thicker than 0.4 m where the ridging activity begins to become significant (Toyota and others, 2007). The lower limit for Equation (1) seems to be ∼0.2 m since below this value the ice-thickening processes are less associated with surface roughness.
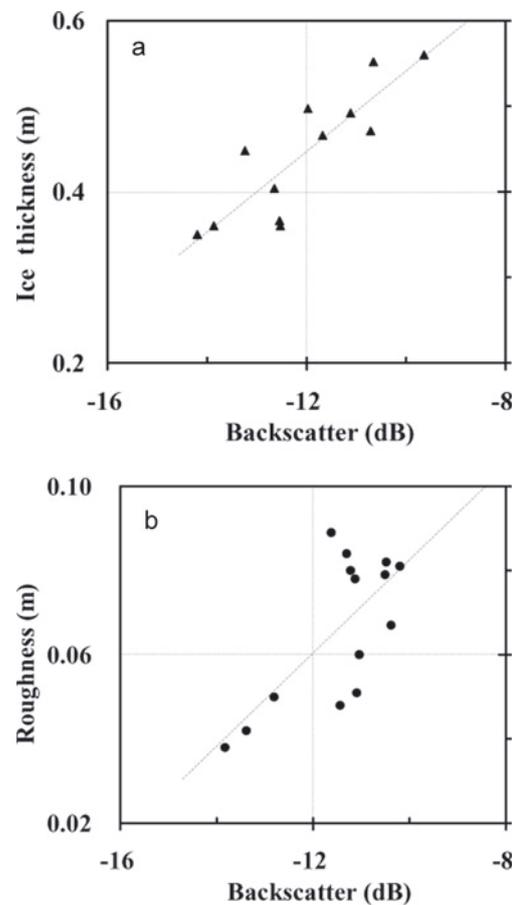
DISCUSSION AND CONCLUSION

Our validation field experiment, coordinated with the spaceborne ALOS/PALSAR overpass, successfully showed that the L-band SAR backscatter coefficients (HH) with a horizontal resolution of 100 m and those obtained with a horizontal resolution of 3 m by the airborne Pi-SAR experiment are similarly correlated with ice thickness and surface roughness. This indicates that satellite L-band backscatter data are a promising tool to estimate ice-thickness distribution in the SIZ, where surface roughness is closely related with the ice-thickness distribution through deformation processes. Additionally, it was found that
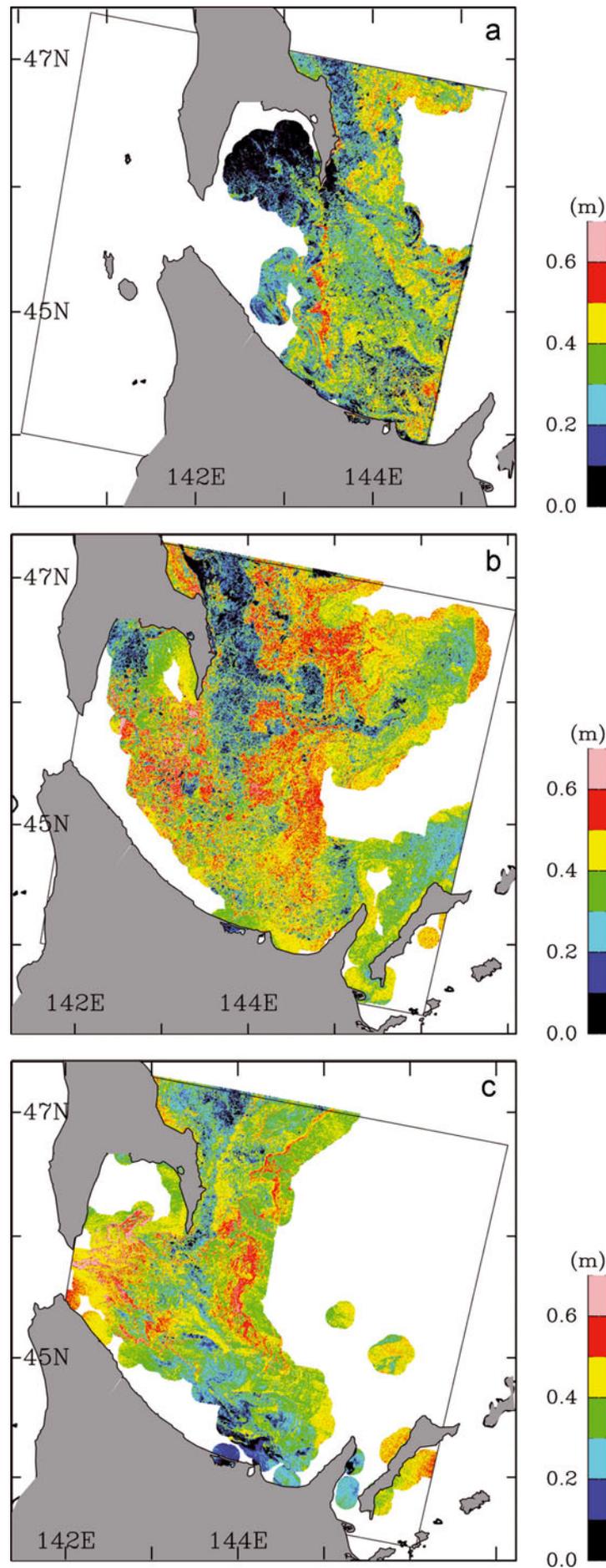
Fig. 4. The pixels of ice thickness (solid black line) and surface roughness (solid red line) used for validation, shown on the map of the backscatter coefficient distribution normalized to the incidence angle of 30.4° (© JAXA). The tracks of ship and helicopter are also depicted with dashed black and red lines, respectively. The region depicted corresponds to the square area in Figure 2a.

heliborne laser profiling can extract surface topography more effectively than a shipborne measurement. Since it has been shown that sea-ice growth processes in this area are similar to those in the Antarctic seas (Toyota and others, 2007), we expect that our results can be applied on the Antarctic sea ice.

To see how the satellite L-band SAR data can represent the ice-thickness distribution in this region, regression (1) is applied to the PALSAR data obtained in mid-February from 2007 to 2009 (Fig. 6). For each image, the dependence of backscatter data on incident angle was calculated individually in the same way, and then the data normalized to the center of the image (30.4°) were supplied to Equation (1). In each figure, the Advanced Scanning Microwave Radiometer (AMSR)-derived ice concentration data were used to extract sea-ice area. We defined the area with ice concentration greater than 15% as sea-ice area, and depicted ice-thickness distribution only for the sea-ice area. Figure 6 shows that in each year ~0.2–0.6 m thick sea ice is dominant and that ice thickness appears to be relatively thicker in 2008 than in 2007 and 2009. The calculated average thicknesses in the southern area (44.3–45.5° N, 142–145° E) are 0.33 ± 0.12, 0.42 ± 0.11 and 0.37 ± 0.11 m. The histogram of ice thickness in each year shows these features more clearly (Fig. 7). This result almost coincides with the observational results. The monitoring of ice-thickness distribution has been conducted with the same video system in the wide area of the southern Sea of Okhotsk in every February since 1996. According to the results of this observation, the average thicknesses are 0.43 ± 0.16, 0.42 ± 0.19 and 0.24 ± 0.16 m in 2007, 2008 and 2009, respectively, indicating significantly thinner ice in 2009. The reason why PALSAR-derived ice thickness in 2007 is much smaller than the observational result may be in part that the thicker area in the eastern side was outside the range in the PALSAR image. Thus PALSAR can be expected to be useful

Fig. 5. Scatter plots of the values averaged for 0.025° segments between (a) normalized backscatter coefficient at HH polarization (incidence angle 30.4°) and ice thickness with a regression line ($r = 0.86$, significant at >99% level); and (b) normalized backscatter coefficient at HH polarization (incidence angle 30.4°) and surface roughness ($r = 0.70$, significant at >99% level).

Fig. 6. PALSAR-derived ice-thickness distributions for (a) 14 February 2007, (b) 12 February 2008 and (c) 14 February 2009 (© JAXA). Only the sea-ice areas (AMSR-derived ice concentration >15%) are depicted.
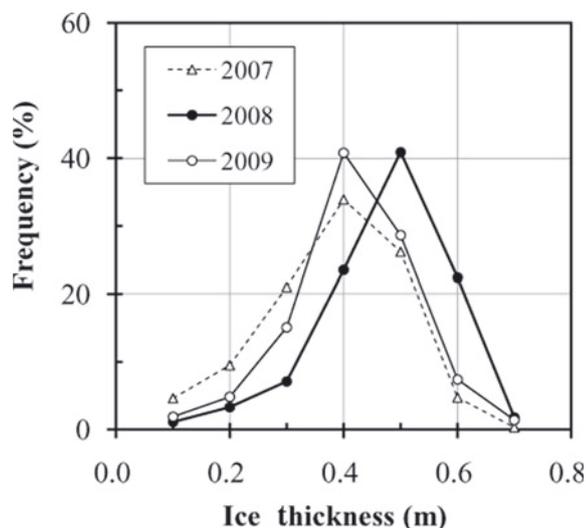
Fig. 7. PALSAR-derived ice-thickness distributions on 14 February 2007, 12 February 2008 and 14 February 2009.

for monitoring the interannual variation of ice thickness, especially for less deformed ice. In addition, characteristic patterns are brought into relief by these figures. On a large scale the thick developed ice extends southward from east of Sakhalin, while on a small scale ice bands near the ice edges in each year and patches of ~0.8 m thick ice floes in the western part in 2008 can be found. These properties will serve to make the ice-thickening processes in each area better understood. We conclude that the retrieval of ice-thickness distribution from PALSAR data seems to be successful in this area.

However, some problems still remain unsolved. One is the effect of open water. Under turbulent conditions, the ocean surface becomes rough and also has high backscatter coefficients even within the sea-ice area. In such a case it is difficult to distinguish between open water and the ice surface with only single polarization SAR data. While in this study we could do this with a video camera, additional information would be required to apply our result to PALSAR data operationally. Moreover, when we extend this result to the polar region, the presence of multi-year ice should be taken into account. Multi-year ice has significantly different properties, in particular in the Arctic. Due to desalination in summer, the penetration depth increases and then the volume scattering becomes more significant at L-band frequencies. In this case, it is known that C-band is more appropriate for distinguishing between multi-year ice and deformed first-year ice (Rignot and Drinkwater, 1994). Therefore, the combination of C- and L-band is desirable. This future work is expected to be accomplished by using L-band SAR effectively together with other satellite sensors.

REFERENCES

Andreas, E.L., M.A. Lange, S.F. Ackley and P. Wadhams. 1993. Roughness of Weddell Sea ice and estimates of the air–ice drag coefficient. *J. Geophys. Res.,* **98**(C7), 12,439–12,452.

Comiso, J.C., P. Wadhams, W.B. Krabill, R.N. Swift, J.P. Crawford and W.B. Tucker, III. 1991. Top/bottom multisensor remote sensing of Arctic sea ice. *J. Geophys. Res.,* **96**(C2), 2693–2709.

Dierking, W. and T. Busche. 2006. Sea ice monitoring by L-band SAR: an assessment based on literature and comparisons of JERS-1 and ERS-1 imagery. *IEEE Trans. Geosci. Remote Sens.,* **44**(4), 957–970.

Fukamachi, Y., G. Mizuta, K.I. Ohshima, T. Toyota, N. Kimura and M. Wakatsuchi. 2006. Sea ice thickness in the southwestern Sea of Okhotsk revealed by a moored ice-profiling sonar. *J. Geophys. Res.,* **111**(C9), C09018. (10.1029/2005JC003327.)

Haas, C. 2003. Dynamics versus thermodynamics: the sea ice thickness distribution. *In* Thomas, D.N. and G.S. Dieckmann, eds. *Sea ice: an introduction to its physics, chemistry, biology and geology.* Oxford, Blackwell, 82–111.

Hibler, W.D., III. 1972. Removal of aircraft altitude variation from laser profiles of the Arctic pack. *J. Geophys. Res.,* **77**(36), 7190–7195.

Ishizu, M., K. Mizutani and T. Itabe. 1999. Airborne freeboard measurements of sea ice and lake ice at the Sea of Okhotsk coast in 1993–95 by a laser altimeter. *Int. J. Remote Sens.,* **20**(12), 2461–2476.

Kern, S., M. Gade, C. Haas and A. Pfaffling. 2006. Retrieval of thin-ice thickness using the L-band polarization ratio measured by the helicopter-borne scatterometer HELISCAT. *Ann. Glaciol.,* **44**, 275–280.

Kimura, N. and M. Wakatsuchi. 1999. Processes controlling the advance and retreat of sea ice in the Sea of Okhotsk. *J. Geophys. Res.,* **104**(C5), 11,137–11,150.

Kurtz, N.T. *and 6 others.* 2009. Estimation of sea ice thickness distributions through the combination of snow depth and satellite laser altimetry data. *J. Geophys. Res.,* **114**(C10), C10007. (10.1029/2009JC005292.)

Kwok, R. and G.F. Cunningham. 2008. ICESat over Arctic sea ice: estimation of snow depth and ice thickness. *J. Geophys. Res.,* **113**(C8), C08010. (10.1029/2008JC004753.)

Kwok, R., H.J. Zwally and D. Yi. 2004. ICESat observations of Arctic sea ice: a first look. *Geophys. Res. Lett.,* **31**(16), L16401. (10.1029/2004GL020309.)

Laxon, S., N. Peacock and D. Smith. 2003. High interannual variability in sea ice thickness in the Arctic region. *Nature,* **425**(6961), 947–950.

Lubin, D. and R. Massom. 2006. Basic remote-sensing principles relating to the measurement of sea ice and its snow cover. *In Polar remote sensing. Volume 1: atmosphere and oceans.* Chichester, Springer-Praxis, 356–380.

Martin, S., R. Drucker, R. Kwok and B. Holt. 2004. Estimation of the thin ice thickness and heat flux for the Chukchi Sea Alaskan coast polynya from Special Sensor Microwave/Imager data. *J. Geophys. Res.,* **109**(C10), C10012. (10.1029/2004JC002428.)

Nakamura, K., H. Wakabayashi, K. Naoki, F. Nishio, T. Moriyama and S. Uratsuka. 2005. Observation of sea-ice thickness in the Sea of Okhotsk by using dual-frequency and fully polarimetric airborne SAR (Pi-SAR) data. *IEEE Trans. Geosci. Remote Sens.,* **43**(11), 2460–2469.

Ohshima, K.I., M. Wakatsuchi, Y. Fukamachi and G. Mizuta. 2002. Near-surface circulation and tidal currents of the Okhotsk Sea observed with satellite-tracked drifters. *J. Geophys. Res.,* **107**(C11), 3195. (10.1029/2001JC001005.)

Rignot, E. and M.R. Drinkwater. 1994. Winter sea-ice mapping from multi-parameter synthetic-aperture radar data. *J. Glaciol.,* **40**(134), 31–45.

Tamura, T., K.I. Ohshima, T. Markus, D.J. Cavalieri, S. Nihashi and N. Hirasawa. 2007. Estimation of thin ice thickness and detection of fast ice from SSM/I data in the Antarctic Ocean. *J. Atmos. Oceanic Technol.,* **24**(10), 1757–1772.

Toyota, T. 2009. Application of remote sensing to the estimation of sea ice thickness distribution. *In* Jedlovec, G., *ed. Advances in geosciences and remote sensing*. Vienna, Intech, 21–44.

Toyota, T., T. Kawamura, K.I. Ohshima, H. Shimoda and M. Wakatsuchi. 2004. Thickness distribution, texture and stratigraphy, and a simple probabilistic model for dynamical thickening of sea ice in the southern Sea of Okhotsk. *J. Geophys. Res.,* **109**(C6), C06001. (10.1029/2003JC002090.)

Toyota, T., S. Takatsuji, K. Tateyama, K. Naoki and K.I. Ohshima. 2007. Properties of thick sea ice and overlying snow in the southern Sea of Okhotsk. *J. Oceanogr.,* **63**(3), 393–411.

Toyota, T., K. Nakamura, S. Uto, K.I. Ohshima and N. Ebuchi. 2009. Retrieval of sea ice thickness distribution in the seasonal ice zone from airborne L-band SAR. *Int. J. Remote Sens.,* **30**(12), 3171–3189.

Uto, S., T. Toyota, H. Shimoda, K. Tateyama and K. Shirasawa. 2006. Ship-borne electromagnetic induction sounding of sea-ice thickness in the southern Sea of Okhotsk. *Ann. Glaciol.,* **44**, 253–260.

Worby, A.P., M.O. Jeffries, W.F. Weeks, R. Morris and R. Jaña. 1996. The thickness distribution of sea ice and snow cover during late winter in the Bellingshausen and Amundsen Seas, Antarctica. *J. Geophys. Res.,* **101**(C12), 28,441–28,455.

Zwally, H.J., D. Yi, R. Kwok and Y. Zhao. 2008. ICESat measurements of sea ice freeboard and estimates of sea ice thickness in the Weddell Sea. *J. Geophys. Res.,* **113**(C2), C02S15. (10.1029/2007JC004284.)